frontiers | Frontiers in Physics

TYPE Original Research
PUBLISHED 09 September 2022
DOI 10.3389/fphy.2022.989047

OPEN ACCESS

EDITED BY
Hainian Han,
Institute of Physics (CAS), China

REVIEWED BY
Marco Lamperti,
University of Insubria, Italy
Kapil Debnath,
Indian Institute of Technology
Kharagpur, India

*CORRESPONDENCE
Ke Yin,
cqyinke@126.com
Tian Jiang,
tjiang@nudt.edu.cn

SPECIALTY SECTION
This article was submitted to Optics and Photonics,
a section of the journal
Frontiers in Physics

RECEIVED 08 July 2022
ACCEPTED 18 August 2022
PUBLISHED 09 September 2022

CITATION
Miao R, Yin K, Zhang C, Yu Z, Cheng X and Jiang T (2022), Stable soliton dual-microcomb generation via sideband thermal compensation for spectroscopy.
Front. Phys. 10:989047.
doi: 10.3389/fphy.2022.989047

Stable soliton dual-microcomb generation *via* sideband thermal compensation for spectroscopy

Runlin Miao[1], Ke Yin[1,2]*, Chenxi Zhang[1], Zhuopei Yu[1], Xiang'ai Cheng[1] and Tian Jiang[1,2]*

[1]College of Advanced Interdisciplinary Studies, National University of Defense Technology, Changsha, China, [2]Beijing Institute for Advanced Study, National University of Defense Technology, Beijing, China

Microcombs—generated by coherently pumping nonlinear microresonators—have emerged as a state-of-the-art scheme at the chip scale. Dual-comb spectroscopy (DCS) technology further takes advantage of the miniature system, and has been demonstrated as a powerful tool for real-time and broadband optical sampling of molecular spectra. Here, a novel soliton dual-microcomb generation method by rapid frequency sweep and sideband thermal compensation is put forward, and dual-microcomb optical spectra range beyond 200-nm has been successfully demonstrated in two microresonators with moderate quality factors. Compared to the dual-microcomb with a weak thermal compensation effect, the demonstrated dual-microcomb shows much lower-noise RF beat notes (<10 kHz) and smaller Allan deviations (1.0×10^{-4} at 1 ms) by increasing sideband power. Moreover, the dual-microcomb has been utilized in the gas absorption detection of $H^{12}CN$ for demonstration with high signal-to-noise ratios (SNRs) and fast acquisition rates. This work also lays a technical foundation for other dual-microcomb applications of ranging and microwave photonics.

KEYWORDS

kerr frequency combs, dual-microcomb, microresonators, soliton, absorption spectroscopy

Introduction

Optical frequency combs [1–3], as a revolutionary technology, have enabled widespread applications in precision spectroscopy [4, 5], frequency metrology [6, 7], communications [8], ranging [9, 10], and optical clocks [11, 12]. The past decade has witnessed the development of chip-scale frequency comb sources utilizing the Kerr nonlinearity in the high-quality-factor (high-Q) microresonators [13–19]. Realization of dissipative Kerr single soliton with high coherent mode-locked state and smooth spectral envelopes has further promoted the application value of microcombs, inspiring vast researches on near-infrared (near-IR) and mid-IR domains with different dielectric material platforms [20–25].

Dual-comb spectroscopy (DCS) [26–28] is a non-intrusive absorption spectroscopy technique without any moving parts. By using two frequency combs with slightly different

repetition rates, DCS technology could enable a mapping from broadband optical molecular absorption spectra into the radio frequency (RF) domain, which can be directly detected by a photodetector (PD). Traditionally, DCS technology has been conducted by mode-locked Ti: sapphire lasers [29, 30], fiber lasers [31–33] and electro-optical (EO) frequency combs [34], which require bulky table-top setups. DCS with microcombs (dual-microcomb spectroscopy) has the capacity for miniaturization and portability. Moreover, the large comb teeth intervals ranging from several gigahertz (GHz) to even above 1 THz enable a large repetition rate difference Δf_{rep}, corresponding to a fast response time for the RF beat notes signals. Suh et al. [35] firstly demonstrated the dual-microcomb spectroscopy in the near-IR domain with two silica disk resonators and then it was then extended to the mid-IR domain by Yu et al. [36] with two silicon microresonators. Recently, Dual-microcomb spectroscopy continues to develop with other material platforms like silicon nitride (Si_3N_4) [37] and other technologies like interleaved difference-frequency-generation [38]. In addition, microcavity-based EO-combs [39] with thin-film lithium niobate technology have also been used for DCS in the near-IR.

However, the simultaneous generation of dual-microcomb with high coherence and miniaturized system is still challenging. Dual-microcomb, consisting of two sets of free-running single soliton microcomb, has a complex system and low relative coherence due to the non-common mode noises from the random drift of pump lasers and temperature variations of two microresonators [35]. Therefore, an approach to ensure high relative coherence by sharing the same pump laser will be critical. Geng et al. [40] and Wang et al. [41] proposed a dual-microcomb generation method by using the auxiliary laser heating [42], in which two auxiliary lasers and other devices like four erbium-doped fiber amplifiers (EDFAs) and four circulators are still needed to balance out the cavity thermal variation and keep the pump laser in the red-detuning regime. Moreover, the Dual-microcomb generation by integrated thermal tuning method [43] could drastically reduce experimental complexity and maintain mutual coherence, but the method has a higher requirement of Q value to overcome the cavity thermal-optic effect.

In this work, a dual-microcomb generation method *via* the combination of rapid frequency sweep with sideband thermal compensation is introduced. In contrast to conventional approaches, this novel scheme possesses a relatively simple system and has a lower requirement on the Q values. The sideband thermal compensation effect caused by a weak modulation of the pump laser improves the mutual coherence, leading to narrower RF beat notes linewidths of <10 kHz and smaller Allan deviations of 1.0×10^{-4} at 1 ms. Furthermore, a proof-of-principle gas absorption spectroscopy measurement of $H^{12}CN$ by the dual-microcomb is performed. The fast acquisition time of 10 μs could realize a mapping from a 5.4-THz optical spectrum span into a 1.5-GHz RF bandwidth with 101.8 GHz resolution without any coherent averaging. When further equipped with field-programmable gate arrays and the coherent averaging algorithm, it will also have the potential for real-time and time-resolved spectral acquisition on microsecond time scales.

Results and discussion

Soliton dual-microcomb generation

Figure 1A shows a simplified schematic of the experimental setup for dual-microcomb spectroscopy, which is divided into a pump unit, a dual-comb generation unit, and a gas detection unit, respectively. The optical part of the pump unit contains a continuous-wave (CW) pump laser at 1549.86 nm, a suppressed-carrier single-sideband modulator (SC-SSBM), and a phase modulator (PM). Then the pump is split into two paths, followed by two EDFAs and two narrow-band (0.5 nm) optical band-pass filters (BPF), and then coupled into two Si_3N_4 microring resonators (MRR), respectively. Si_3N_4 has been proved to be a favorable platform benefiting from the ultra-low linear loss, wide transparency windows, high nonlinear index ($n_2 \sim 2.4 \times 10^{-19}$ m^2/W), and manageable optional group velocity dispersion (GVD) by tailoring the waveguide geometry. The waveguides of MRRs have the same cross-section of 800 nm × 1600 nm to guarantee the anomalous GVD condition at 1549.86 nm. The radii of the two resonators are designed to be the same as 221.15 μm, corresponding to a free spectral range (FSR) of 101.8 GHz for the transverse magnetic (TM_{00}) mode. Due to the fabrication errors, the same radii introduce an FSR offset of tens of MHz, which is suited for precise measurement applications such as spectroscopy and ranging.

Figures 1B,C show the transmission spectra of the two soliton modes in two MRRs. The full width at half maxima (FWHM) linewidths can be extracted by fitting with Lorentzian lineshapes, which are measured to be 183 and 167 MHz, corresponding to moderate loaded Q factors of 1.05 million and 1.15 million, respectively. To create a miniature and coherent dual-comb system, both microcombs are necessarily generated by a common pump laser, which means that the soliton modes of two MRRs need to be aligned to the pump mode. Therefore, thermo-electric coolers (TECs) were packaged beneath the MRRs for coarsely tuning the resonance wavelength with a resolution of 0.01°C according to the thermo-optic effect. Figure 2A shows the mode transmission spectra of MRR1 and MRR2 at low pump power and different temperatures. The temperature of MRR2 is firstly set to be 18.30°C to match the soliton mode with the pump laser wavelength. Next, the effective control of the soliton mode variation of MRR1 is shown by tuning the TEC temperature. As the temperature is increased from 15 to 45°C, a resonance wavelength red-shift can be observed from 1549.33 nm to

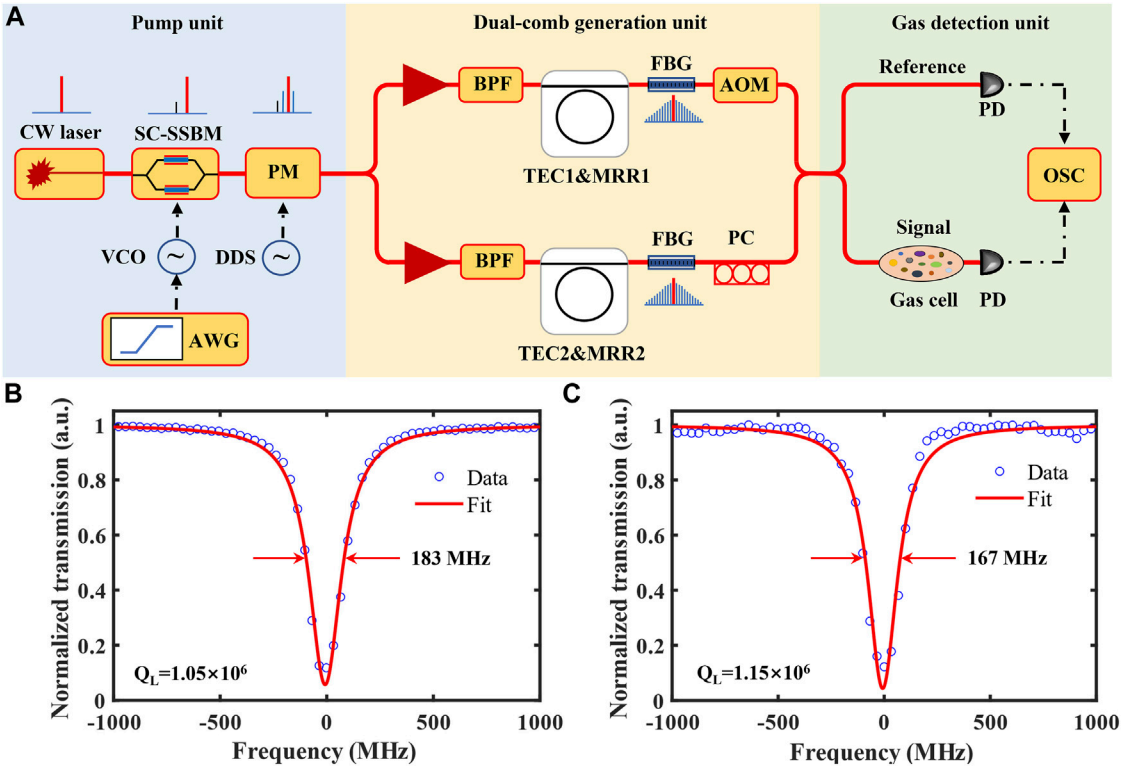

FIGURE 1
Experimental setup for dual-microcomb generation for spectroscopy. **(A)** Schematic of the experimental setup. SC-SSBM, suppressed-carrier single-sideband modulator; VCO, voltage-controlled oscillator; AWG, arbitrary waveform generator; PM, phase modulator; DDS, direct digital synthesis; BPF, band-pass filter; TEC, thermo-electric cooler; MRR, microring resonator; FBG, fiber Bragg grating; AOM, acousto-optic modulator; PC, polarization controller; PD, photodetector; OSC, oscilloscope; **(B,C)** are transmission spectra and Lorentzian fits for Q-factors measurements of two MRRs' soliton modes, respectively.

1550.01 nm. Figure 2B depicts the relation between the chip temperature and the resonance wavelength, with a linear fitting slope $d\lambda/dT$ of 0.0227 nm/K, which is consistent with the result in Ref. [44]. Therefore, when the temperature of MRR1 is set at 35°C, the soliton modes of MRR1 and MRR2 and the pump laser can achieve wavelength alignment.

As for the dual-microcomb generation, the method by combining the rapid frequency sweep with the sideband thermal compensation [45] is adopted. Compared to the auxiliary laser heating and integrated thermal tuning methods, this method shows a relatively simple system and a lower requirement on the Q values, respectively, by overcoming the thermal effect of the cavity and enlarging the "soliton existence range". Here, the soliton existence range is defined as the frequency range that the pump laser can be swept without losing the soliton microcombs. To be specific, a rapid voltage ramp of 4–8 V through an arbitrary waveform generator (AWG) is applied to the voltage-controlled oscillator (VCO) driving the SSBM, corresponding to a rapid suppressed-carrier single-sideband frequency scanning of approximately 2.08 GHz within 75 ns from short to long wavelength. This rapid scanning speed of 27.25 GHz/μs, close to the thermo-optic response time of Si_3N_4 microresonators, could satisfy the equilibrium condition of the single-soliton microcomb generation. Then, an RF signal from the direct digital synthesis (DDS) with power and frequency of 6 dBm and 1000 MHz, respectively, is modulated on the phase modulator (PM) to generate an effective blue-shifted optical sideband, which plays a vital role in the cavity thermal compensation effect. As shown in Ref. [45], firstly, it could increase the "soliton existence range" from more than one hundred MHz to several GHz and reduce the pump power requirement. Secondly, the blue-shifted sideband is located in the thermal self-lock region, and could improve the soliton microcomb existence time from 1 h to beyond 12 h. Third, the sideband thermal compensation could effectively counteract thermo-refractive noise and achieve enhanced repetition rate stability and a decrease in the effective linewidth of the microcomb lines, which is also important for dual-microcomb performance.

On-chip pump powers of about 688 mW (MRR1) and 800 mW (MRR2) are needed for dual-microcomb generation. Then at the MRRs' output, two microcombs are then sent to two

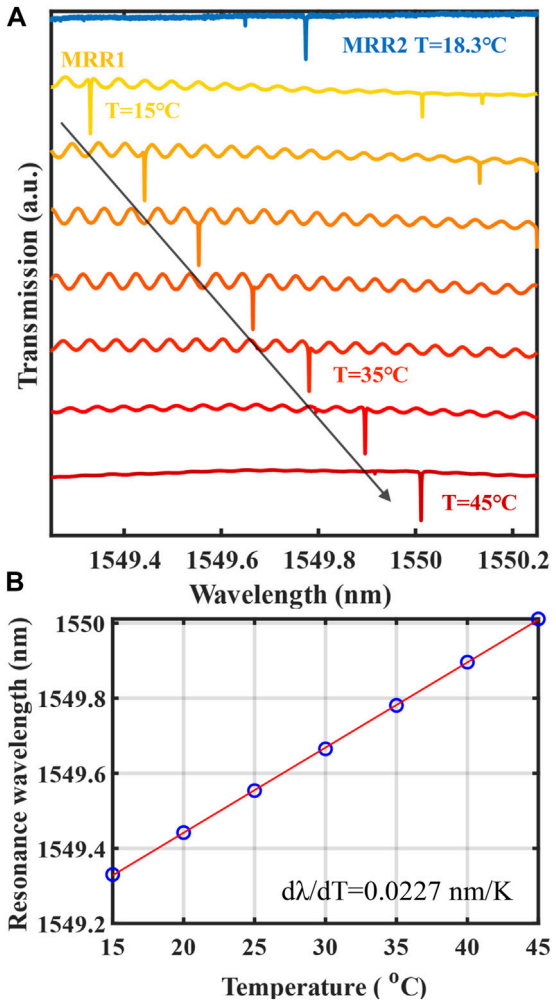

FIGURE 2
(A) Transmission of the two different soliton modes at low power and different temperatures. **(B)** Dependence of the resonance wavelength on the chip temperature and a linear fit.

fiber-Bragg gratings (FBGs) to exclude the strong pump for soliton outputs and monitoring. The calculated soliton conversion efficiencies are about 0.65 and 0.58%, respectively. Figure 3A illustrates the microcomb soliton powers evolution process when the control signal to scan the pump laser wavelength is applied. The soliton steps confirm that the microcombs go through the chaotic state and finally stay in the single-soliton state. There is a drift between the control signal and the detected onset of chaos/soliton dynamics, which could be possibly ascribed to the delayed response of the VCO. Figure 3B shows the generated dual single-soliton microcombs spectra spanning over 200 nm (25 THz). The spectra are well fitted by the $sech^2$ function and the 3 dB bandwidth of the spectrum is around 40.5 nm, corresponding to a Fourier-transform-limited pulse duration of 62 fs.

Due to the thermal compensation effect [46], the modulated blue detuned pump sideband can stay in the thermal self-lock region and help mitigate the resonance frequency shift caused by the environmental thermal variation. Therefore, the dual-microcomb could stably stay for several hours with no active locking technique used in experiments. Figure 3D shows the optical spectrum evolution map over 2.5 h between 1635.8 nm and 1637 nm. The spectra range is selected because the small repetition difference of tens of MHz cannot be directly distinguished at the spectrum center location with the spectrometer resolution of 0.02 nm. The comb line spacing determines the resolution of the dual-microcomb spectroscopy and the repetition rate difference is relevant to the spectroscopy acquisition speed. The repetition rate measurements are conducted by linear fitting the spectrum data obtained from the high precision spectrometer with a resolution of 0.04 p.m. As shown in Figure 3C, the two fits give estimations of the microcomb line spacings of 101.7424 and 101.7707 GHz for Comb1 and Comb2, respectively. Therefore, the repetition rate difference is obtained to be about 28.3 MHz, which indicates that a series of down-converting RF lines will arrange at this interval in DCS detection.

Radio frequency beat notes characterization

In order to have a better understanding of the repetition rate difference performance, the first red-detuned pair (around 1550.68 nm) of the comb teeth with respect to the pump is filtered out and detected by a PD. It is found that the repetition rate difference has a variation of approximately 1 MHz centered at 28 MHz at different pump powers. As demonstrated in Ref. [45], the modulated sideband plays a significant role in thermal compensation, which can effectively counteract thermo-refractive noise and achieve enhanced repetition rate stability. Hence, a better repetition rate difference beat note stability of the dual-microcomb is also predictable. For demonstration, the repetition rate difference characterization is compared with two different RF modulation powers of 0 dBm and 6 dBm, respectively in Figure 4. The dual-microcomb with RF power of 0 dBm is acquired by slowly tuning the pump laser wavelength while reducing the RF power from 6 dBm to 0 dBm. Unfortunately, one of the dual-microcomb collapses due to the decreased "soliton existence range" when the RF power is further decreased, though it can be realized in the single microcomb system. Therefore, a complete free-running dual-comb without the modulated sideband is not realized. The dual-microcomb with the 0-dBm modulation signal also has a shorter soliton existence time of about only several minutes, which is far less than that with modulation signal power of 6 dBm. Moreover, when the RF modulation power is increased beyond 6 dBm, the sideband power would exceed the parametric oscillation

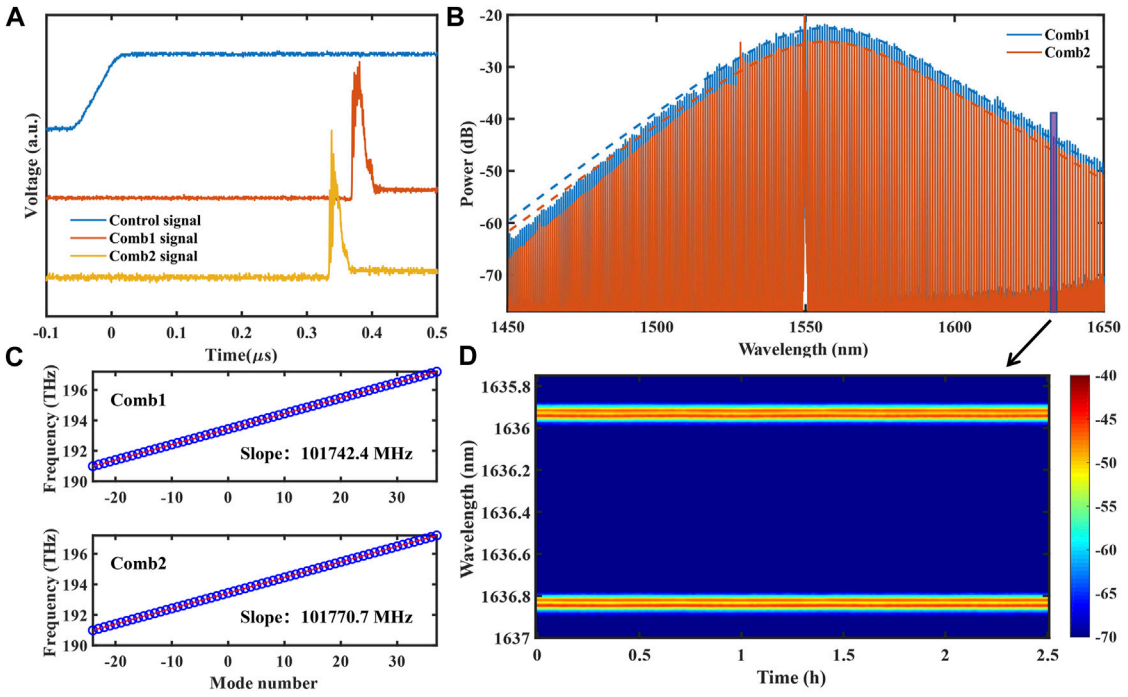

FIGURE 3
Soliton dual-microcomb generation and characterization. **(A)** Observed soliton steps versus scan time in the OSC. The blue curve represents the control signal of AWG to drive the VCO. The red and yellow curves show the power traces of the two soliton microcombs excluding the pump power. **(B)** Generated two single-soliton mode-locked microcomb optical spectra. Two fitted sech^2 envelopes are also indicated by the blue and red dotted lines. **(C)** Characterization of two comb spacings over 60 comb lines and two linear fits. **(D)** Optical spectrum evolution color map beyond 2.5 h between 1635.8 nm and 1637 nm. The color bar reflects the power amplitude in the unit of decibel-milliwatts (dBm).

threshold (measured about 70 mW) and hinder the single soliton generation.

Figure 4A shows the measurements of the repetition rate difference drift within 5 min through a frequency counter at 1 ms gate time. The blue points represent the signal of the weakly modulated sideband, which has a jittering scope of about 700 kHz and a standard deviation (SD) of 107 kHz. The dual-microcomb with a higher modulated sideband power has a much less frequency drifting range of about 200 kHz and a SD of 35.4 kHz. Allan deviations have also been calculated in Figure 4C, which are subject to the environment temperature fluctuation and pump laser frequency drift in the free-running system. The instability is 3.1×10^{-4} at 1 ms for the dual-microcomb with lower RF modulation power, while there is a threefold decrease (1.0×10^{-4} at 1 ms) by injecting stronger sideband power due to the enhanced microcomb repetition rate stability, which is close to the stability in the Ref. [47]. It is also found that the Allan deviations would have a declining trend beyond 1 s integration time, which may be caused by the thermal compensation effect that reduces the long-time relative drift between the dual-microcomb.

The soliton mode-locked dual-microcomb has repetition rate difference beat notes with 3-dB linewidths of about 20 kHz and less than 10 kHz for RF modulation signals of 0 dBm and 6 dBm, respectively (Figure 4B). The stronger sideband power with narrower beat note (<10 kHz) guarantees a longer relative coherence time ($\tau_{rel} = 1/(10\,\text{kHz}) = 100\,\mu\text{s}$), which means that a longer time-domain signal sequence can be acquired from the oscilloscope (OSC). Note that the high relative coherence of the dual-microcomb comes from the same low-noise pump laser and the effective sideband thermal compensation effect, although the combs are free-running.

Time-domain interferogram

Next, a simple demonstration for the dual-microcomb spectroscopy application is conducted in experiments. Owing that the dual-microcomb shares the same pump laser, the down-converted RF spectrum of the left and right wings of the optical spectrum would be mixed up and cannot be distinguished. Therefore, as shown in Figure 1A, one of the microcombs at the dual-comb generation unit is sent to an acousto-optic modulator (AOM) to shift the spectrum of Comb1 with the f_{AOM} of 80 MHz, and the other microcomb goes through the polarization controller (PC) to maximize the interference signal.

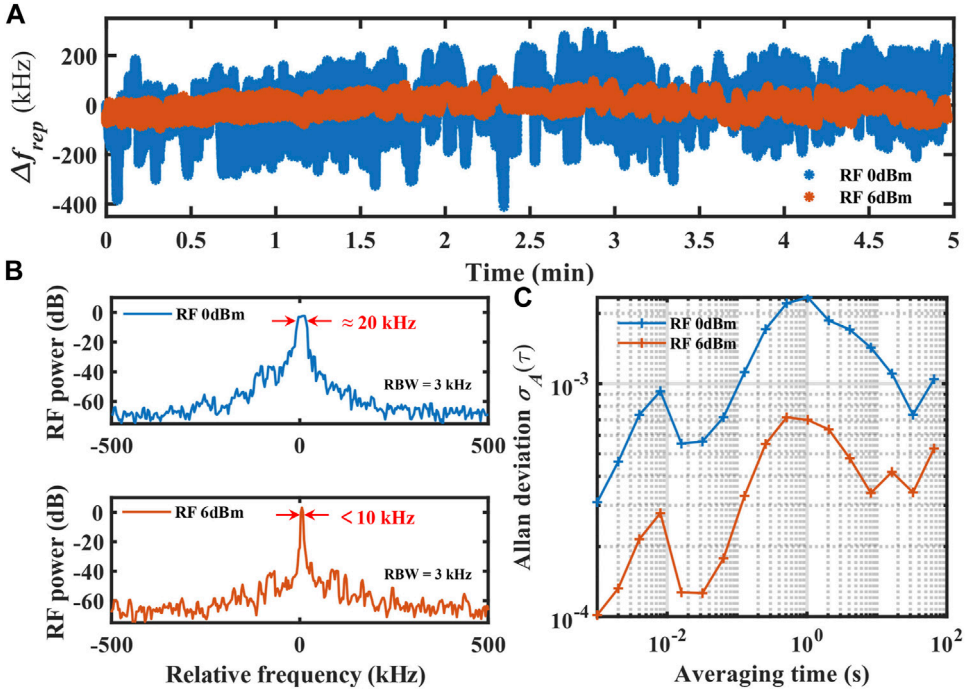

FIGURE 4
Repetition rate difference characterization of free-running dual-microcomb with different sideband modulation powers of 0 dBm (blue dots and lines) and 6 dBm (red dots and lines), respectively. **(A)** Repetition rate difference frequency counting measurement within 5 min at 1 ms gate time. **(B)** Repetition rate difference beat notes measured by the RF spectrum analyzer. The sweep time is set as 33.8 ms within a sweep range of 1 MHz with a resolution bandwidth (RBW) of 3 kHz. **(C)** Allan deviations of the repetition rate difference signal.

Figure 5A depicts the schematic of the dual-microcomb optical spectrum and down-converted electrical spectrum mapping after the frequency shift. The RF beat notes of the dual-microcomb spectrum in the longer wavelength appear at frequencies $f_N = 80\,\text{MHz} + N \times \Delta f_{\text{rep}}$, and the RF beat notes on the shorter wavelength appear at frequencies $f_N = |80\,\text{MHz} - N \times \Delta f_{\text{rep}}|$, where N is an integer.

After combining the dual-microcomb with a fiber bidirectional coupler, one output passes through the test sample (gas cell) to serve as a signal output and the other acts as a reference output. Both outputs are synchronously detected with photodetectors and a fast real-time OSC to generate two interferograms of the two soliton pulse trains. Figure 5B shows an interferogram of the signal path within 10 μs at 5 gigasamples/s due to the maximum record length limitation of the OSC, though it is smaller than the maximum coherence time (>100 μs) of the dual-microcomb. The lower panel displays a zoomed-in time-domain interferogram result from −0.1 to 0.4 μs. The small period waveform repeats every 35.7 ns, corresponding to the inverse of the difference frequency (28 MHz) in the dual-microcomb repetition rates. It should also be emphasized that the maximum period lasts for 250 ns, corresponding to the inverse of the RF signal of 4 MHz from the beat note of the third pair of the dual-microcomb on the shorter wavelength. This maximum period also represents that the dual-microcomb system has a short single-shot acquisition time.

The time-domain interferogram is then Fourier-transformed to produce a comb-like RF electrical spectrum in Figure 5C. The beat-note signals of the two sides of the dual-microcomb spectrum are unaligned around the center frequency of f_{AOM} (80 MHz), though the 80-MHz frequency cannot be detected owing to the filtered pump of the dual-microcomb. The RF comb lines of each side of the spectrum have a line spacing of 28 MHz by the repetition rate difference of the soliton pulse trains. The small repetition rate difference compared to the 101.8 GHz soliton microcomb repetition rate makes it feasible to compress an optical span of 5.4 THz (1505–1590 nm) into 1500 MHz of electrical spectrum. The electrical spectrum has over 100 RF teeth and the intensity profile agrees well with the product of the amplitudes of the electric fields of the dual-microcomb. The RF lines near the 80 MHz frequency have high signal-to-noise ratios (SNRs) around 27 dB. However, we have also found some unwanted RF lines such as the modulated 1 GHz signal for dual-microcomb generation and some sum and difference frequency signals between the dual-microcomb beat notes and the 1 GHz signal. Fortunately, the unwanted RF lines are not overlapped with the dual-microcomb beat notes and have no effect on the experiment except for a slight reduction in SNRs.

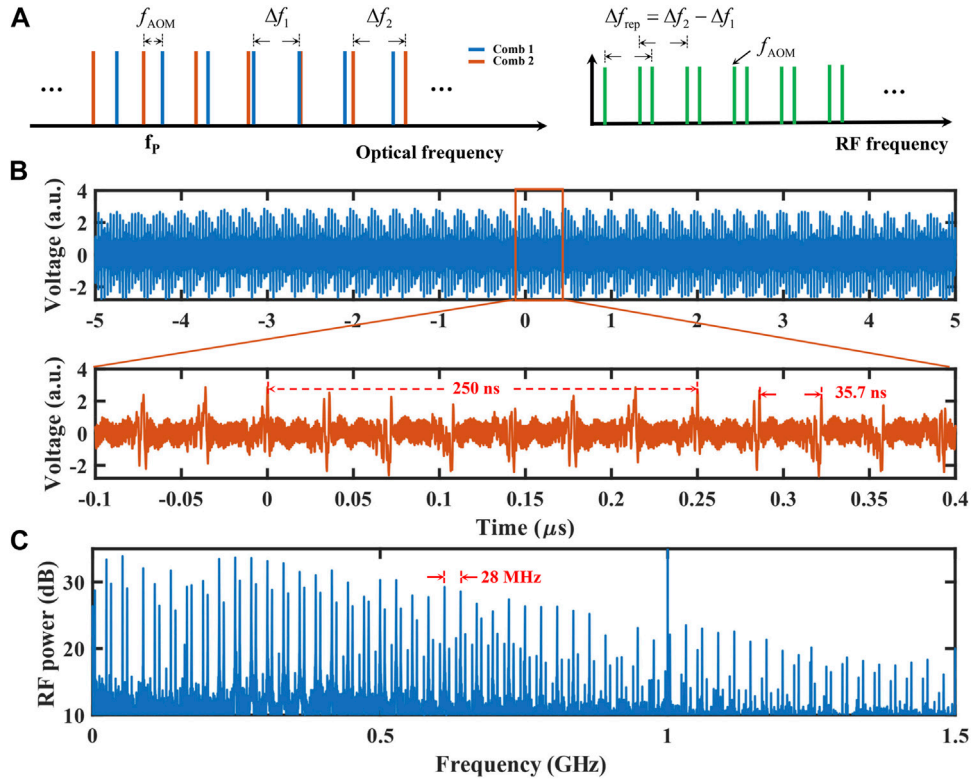

FIGURE 5
Experimental interferogram sequence and RF spectrum. **(A)** Schematic for dual-microcomb spectrum in optical domain and RF domain. Δf_1 and Δf_2 are the repetition rates of two microcombs. $\Delta f_{rep} = \Delta f_2 - \Delta f_1$ is the difference frequency in repetition rates. f_{AOM} is the frequency shift of the AOM. **(B)** Time-domain interferogram results of the dual-microcomb soliton pulses with the acquisition time of 10 μs. **(C)** The Fourier-transformed electrical spectrum of the time-domain signal.

Proof-of-principle gas spectroscopy measurement

The dual-microcomb source has a short single spectrum acquisition time of about 250 ns at the expense of coarse resolution (101.8 GHz), which is suitable for liquids or solids detection with broad absorption features. However, limited by the experimental conditions, only a simple proof-of-principle gas absorption spectroscopy detection as an alternative in Figure 6A is performed. The gas cell used here has a mixture of $H^{12}CN$, ^{12}CO and ^{13}CO, and the pressures of the gases inside the cell are 10 Torr ($H^{12}CN$), 300 Torr (^{12}CO) and 300 Torr (^{13}CO), respectively. The blue lines represent the reference absorption spectrum obtained by conducting a wavelength scanning from 1522 nm to 1569 nm with an external cavity diode laser (ECDL). The output from the ECDL is split into three paths. One is coupled into the gas cell, another is used for monitoring the power fluctuation, and the last one is injected into the fiber ring with FSR at about 34 MHz for accurate wavelength calibration. The red lines are the results of the dual-microcomb spectroscopy, which is extracted by normalizing the signal spectrum by the reference spectrum. Here, only 10 μs time-domain signals are processed without any complex coherent averaging on multiple spectra, thus indicating the real-time nature of the dual-microcomb acquisition system.

Then the results of both absorption spectra on the upper panel in Figure 6A are compared. Owing that the coarse resolution of the dual-microcomb system (~101.8 GHz) is much larger than the gas absorption linewidth of ~21 GHz, the absorption of ^{12}CO in the longer wavelength cannot be distinguished and only several absorption lines of $H^{12}CN$ on the shorter wavelength are coincidently detected. Other microcomb lines that miss the absorption lines can also measure the baseline absorption variations well. Furthermore, the line-by-line overlay of the wavelength-calibrated scanning laser spectrum and dual-comb spectrum on the lower panel in Figure 6A shows a clearer comparation of absorption intensity for $H^{12}CN$ from 1522 nm to 1533 nm. Most of the microcomb lines have a close strength compared to the reference except for some large deviations of individual microcomb lines, which are primarily limited by the short measurement time and low SNR in the wings of dual-microcomb spectrum. Moreover, the extra unwanted RF lines

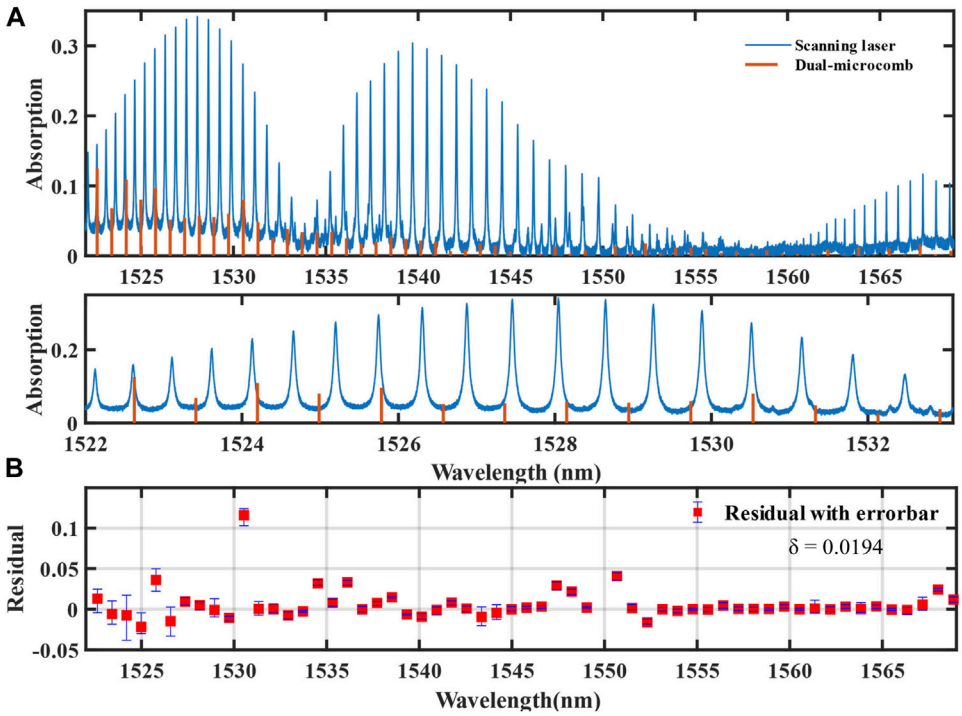

FIGURE 6
Gas absorption spectra test. **(A)** The gas absorption spectra measured by the wavelength-calibrated scanning laser and dual-microcomb. The absorption is defined as 1−T, with T the transmittance of the gas cell. The lower panel represents the spectra range between 1522 nm and 1533 nm. **(B)** The residual difference with errorbar between the two spectra.

caused by the 1 GHz modulation signals would further reduce the overall SNR. After averaging several time-domain results, the residual difference with errorbar between the two absorption spectra is shown in Figure 6B and the calculated SD is 0.0194, which is comparable with that in Ref. [35]. It is believed that coherent averaging over abundant acquisitions can reduce the deviations, but at the cost of a longer acquisition time. Supplementary Table S1 provides a comparison of dual-microcomb parameters between our work and previous references.

Conclusion

In conclusion, a stable dual-microcomb generation method by utilizing the sideband thermal compensation effect has been demonstrated with two Si_3N_4 microresonators. Narrower repetition rate difference beat notes (<10 kHz) and smaller Allan deviations (1.0×10^{-4} at 1 ms) are achieved. This system has no strict requirement for ultra-high Q microrings and shows great potential for miniaturization and integration with compact and portable compositions. Moreover, the repetition rate difference Δf_{rep} of 28 MHz would map over 100 microcomb lines from an optical span of 5.4 THz (1505–1590 nm) with 101.8 GHz resolution into the 1.5-GHz RF bandwidth. A simple gas absorption detection of $H^{12}CN$ has been demonstrated. In principle, a dual-microcomb source with a higher-resolution ability (i.e., lower repetition rate) is more suitable for accurate gas absorption peaks detection and a real-time coherent averaging with field-programmable gate arrays could be adopted to reduce the residual. Moreover, the dual-microcomb framework is also suitable for other dual-comb technology requirements for ranging and microwave photonics.

Data availability statement

The raw data supporting the conclusion of this article will be made available by the authors, without undue reservation.

Author contributions

KY and TJ conceived the idea. RM and ZY performed the experiments. RM and CZ conducted the data processing. RM, KY, and XC contributed to writing and editing the paper. All authors have approved the final version of the manuscript.

Funding

This work was supported by the National Key Research and Development Program of China (2020YFB2205804), National Natural Science Foundation of China (62075240), Science Fund for Distinguished Young Scholars of Hunan Province (2020JJ2036), and Postgraduate Scientific Research Innovation Project of Hunan Province (CX20210004).

Conflict of interest

The authors declare that the research was conducted in the absence of any commercial or financial relationships that could be construed as a potential conflict of interest.

Publisher's note

Supplementary material

The Supplementary Material for this article can be found online at: https://www.frontiersin.org/articles/10.3389/fphy.2022.989047/full#supplementary-material

References

1. Diddams SA, Vahala K, Udem T. Optical frequency combs: Coherently uniting the electromagnetic spectrum. *Science* (2020) 369:eaay3676. doi:10.1126/science.aay3676

2. Zhang H, Chang B, Li Z, Liang Y, Qin C, Wang C, et al. Coherent optical frequency combs: From principles to applications. *J Electron Sci Technology* (2022) 20:100157. doi:10.1016/j.jnlest.2022.100157

3. Wang H, Han H, Zhang Z, Shao X, Zhu J, Wei Z. An yb-fiber frequency comb phase-locked to microwave standard and optical reference. *Chin Phys B* (2020) 29:030601. doi:10.1088/1674-1056/ab696d

4. Chen Z, Hansch TW, Picque N. Mid-infrared feed-forward dual-comb spectroscopy. *Proc Natl Acad Sci U S A* (2019) 116:3454–9. doi:10.1073/pnas.1819082116

5. Niu R, Wan S, Li J, Zhao R, Zou C, Guo G, et al. Fast spectroscopy based on a modulated soliton microcomb. *IEEE Photon J* (2021) 13:1–4. doi:10.1109/jphot.2021.3104934

6. Hall JL. Nobel lecture: Defining and measuring optical frequencies. *Rev Mod Phys* (2006) 78:1279–95. doi:10.1103/RevModPhys.78.1279

7. Shen Q, Guan J, Zeng T, Lu Q, Huang L, Cao Y, et al. Experimental simulation of time and frequency transfer via an optical satellite–ground link at 10-18 instability. *Optica* (2021) 8:471. doi:10.1364/optica.413114

8. Marin-Palomo P, Kemal JN, Karpov M, Kordts A, Pfeifle J, Pfeiffer MHP, et al. Microresonator-based solitons for massively parallel coherent optical communications. *Nature* (2017) 546:274–9. doi:10.1038/nature22387

9. Riemensberger J, Lukashchuk A, Karpov M, Weng W, Lucas E, Liu J, et al. Massively parallel coherent laser ranging using a soliton microcomb. *Nature* (2020) 581:164–70. doi:10.1038/s41586-020-2239-3

10. Mitchell T, Sun J, Reid DT. Dynamic measurements at up to 130-khz sampling rates using ti:Sapphire dual-comb distance metrology. *Opt Express* (2021) 29:42119. doi:10.1364/oe.433871

11. Papp SB, Beha K, Del'Haye P, Quinlan F, Lee H, Vahala KJ, et al. Microresonator frequency comb optical clock. *Optica* (2014) 1:10–4. doi:10.1364/optica.1.000010

12. Zhang P, Zhang Y, Li M, Rao B, Yan L, Chen F, et al. All polarization-maintaining er:Fiber-based optical frequency comb for frequency comparison of optical clocks. *Chin Phys B* (2022) 31:054210. doi:10.1088/1674-1056/ac40f6

13. Chang L, Liu S, Bowers JE. Integrated optical frequency comb technologies. *Nat Photon* (2022) 16:95–108. doi:10.1038/s41566-021-00945-1

14. Wang W, Wang L, Zhang W. Advances in soliton microcomb generation. *Adv Photon* (2020) 2:034001. doi:10.1117/1.Ap.2.3.034001

15. Ma J, Xiao L, Gu J, Li H, Cheng X, He G, et al. Visible kerr comb generation in a high-q silica microdisk resonator with a large wedge angle. *Photon Res* (2019) 7:573–8. doi:10.1364/prj.7.000573

16. Wan S, Niu R, Wang Z-Y, Peng J, Li M, Li J, et al. Frequency stabilization and tuning of breathing solitons in si3n4 microresonators. *Photon Res* (2020) 8:1342–9. doi:10.1364/prj.397619

17. Hu Y, Ding S, Qin Y, Gu J, Wan W, Xiao M, et al. Generation of optical frequency comb via giant optomechanical oscillation. *Phys Rev Lett* (2021) 127:134301. doi:10.1103/PhysRevLett.127.134301

18. Bai Y, Zhang M, Shi Q, Ding S, Qin Y, Xie Z, et al. Brillouin-kerr soliton frequency combs in an optical microresonator. *Phys Rev Lett* (2021) 126:063901. doi:10.1103/PhysRevLett.126.063901

19. Zhang Q, Liu B, Wen Q, Qin J, Geng Y, Zhou Q, et al. Low-noise amplification of dissipative kerr soliton microcomb lines via optical injection locking lasers. *Chin Opt Lett* (2021) 19:121401. doi:10.3788/col202119.121401

20. Wan S, Niu R, Peng J, Li J, Guo G, Zou C, et al. Fabrication of the high-q si_3n_4 microresonators for soliton microcombs. *Chin Opt Lett* (2022) 20:032201. doi:10.3788/col202220.032201

21. Weng H, Liu J, Afridi AA, Li J, Dai J, Ma X, et al. Directly accessing octave-spanning dissipative kerr soliton frequency combs in an aln microresonator. *Photon Res* (2021) 9:1351–7. doi:10.1364/prj.427567

22. Shu H, Chang L, Tao Y, Shen B, Xie W, Jin M, et al. Microcomb-driven silicon photonic systems. *Nature* (2022) 605:457–63. doi:10.1038/s41586-022-04579-3

23. Wang X, Xie P, Wang W, Wang Y, Lu Z, Wang L, et al. Program-controlled single soliton microcomb source. *Photon Res* (2020) 9:66–72. doi:10.1364/prj.408612

24. Yao L, Liu P, Chen H, Gong Q, Yang Q, Xiao Y. Soliton microwave oscillators using oversized billion q optical microresonators. *Optica* (2022) 9:561. doi:10.1364/optica.459130

25. Wen Q, Cui W, Geng Y, Zhou H, Qiu K. Precise control of micro-rod resonator free spectral range via iterative laser annealing. *Chin Opt Lett* (2021) 19:071903. doi:10.3788/col202119.071903

26. Coddington I, Newbury N, Swann W. Dual-comb spectroscopy. *Optica* (2016) 3:414–26. doi:10.1364/optica.3.000414

27. Picqué N, Hänsch TW. Frequency comb spectroscopy. *Nat Photon* (2019) 13:146–57. doi:10.1038/s41566-018-0347-5

28. Kara O, Maidment L, Gardiner T, Schunemann PG, Reid DT. Dual-comb spectroscopy in the spectral fingerprint region using opgap optical parametric oscillators. *Opt Express* (2017) 25:32713. doi:10.1364/oe.25.032713

29. Ideguchi T, Nakamura T, Kobayashi Y, Goda K. Kerr-lens mode-locked bidirectional dual-comb ring laser for broadband dual-comb spectroscopy. *Optica* (2016) 3:748. doi:10.1364/optica.3.000748

30. Liu H, Sun S, Zheng L, Wang G, Tian W, Zhang D, et al. Review of laser-diode pumped ti:Sapphire laser. *Microw Opt Technol Lett* (2021) 63:2135–44. doi:10.1002/mop.32882

31. Chen Z, Yan M, Hansch TW, Picque N. A phase-stable dual-comb interferometer. *Nat Commun* (2018) 9:3035. doi:10.1038/s41467-018-05509-6

32. Guo H, Weng W, Liu J, Yang F, Hänsel W, Brès CS, et al. Nanophotonic supercontinuum-based mid-infrared dual-comb spectroscopy. *Optica* (2020) 7:1181. doi:10.1364/optica.396542

33. Yan Q, Li Y, Zhang J, Zheng X, Wu D, Yin K, et al. A free-running dual-comb spectrometer with intelligent temporal alignment algorithm. *Opt Laser Technol* (2021) 141:107175. doi:10.1016/j.optlastec.2021.107175

34. Durán V, EscobarVera C, SorianoAmat M, Martins HF, MartinLopez S, GonzalezHerraez M, et al. Dual electro-optic comb spectroscopy using a single pseudo-randomly driven modulator. *Opt Express* (2022) 30:25103. doi:10.1364/oe.463604

35. Suh M-G, Yang Q-F, Yang KY, Yi X, Vahala K. Microresonator soliton dual-comb spectroscopy. *Science* (2016) 354:600–3. doi:10.1126/science.aah6516

36. Yu M, Okawachi Y, Griffith AG, Picque N, Lipson M, Gaeta AL. Silicon-chip-based mid-infrared dual-comb spectroscopy. *Nat Commun* (2018) 9:1869. doi:10.1038/s41467-018-04350-1

37. Dutt A, Joshi C, Ji X, Cardenas J, Okawachi Y, Luke K, et al. On-chip dual-comb source for spectroscopy. *Sci Adv* (2018) 4:e1701858. doi:10.1126/sciadv.1701858

38. Bao C, Yuan Z, Wu L, Suh MG, Wang H, Lin Q, et al. Architecture for microcomb-based ghz-mid-infrared dual-comb spectroscopy. *Nat Commun* (2021) 12:6573. doi:10.1038/s41467-021-26958-6

39. Shams-Ansari A, Yu M, Chen Z, Reimer C, Zhang M, Picqué N, et al. Thin-film lithium-niobate electro-optic platform for spectrally tailored dual-comb spectroscopy. *Commun Phys* (2022) 5:88–8. doi:10.1038/s42005-022-00865-8

40. Geng Y, Zhou H, Han X, Cui W, Zhang Q, Liu B, et al. Coherent optical communications using coherence-cloned kerr soliton microcombs. *Nat Commun* (2022) 13:1070–8. doi:10.1038/s41467-022-28712-y

41. Wang Y, Wang Z, Wang X, Shao W, Huang L, Liang B, et al. Scanning dual-microcomb spectroscopy. *Sci China Phys Mech Astron* (2022) 65:294211–7. doi:10.1007/s11433-022-1920-6

42. Zhou H, Geng Y, Cui W, Huang SW, Zhou Q, Qiu K, et al. Soliton bursts and deterministic dissipative kerr soliton generation in auxiliary-assisted microcavities. *Light Sci Appl* (2019) 8:50–10. doi:10.1038/s41377-019-0161-y

43. Lin T, Dutt A, Joshi C, Ji X, Phare CT, Okawachi Y, et al. *Broadband ultrahigh-resolution chip-scale scanning soliton dual-comb spectroscopy. arXiv preprint arXiv: 00869* (2020).

44. Weng H, Afridi AA, Li J, McDermott M, Tu H, Barry LP, et al. Dual-mode microresonators as straightforward access to octave-spanning dissipative kerr solitons. *APL Photon* (2022) 7:066103. doi:10.1063/5.0089036

45. Miao R, Zhang C, Zheng X, Cheng X, Yin K, Jiang T. Repetition rate locked single-soliton microcomb generation via rapid frequency sweep and sideband thermal compensation. *Photon Res* (2022) 10:1859–67. doi:10.1364/prj.458472

46. Nishimoto K, Minoshima K, Yasui T, Kuse N. Thermal control of a kerr microresonator soliton comb via an optical sideband. *Opt Lett* (2022) 47:281–4. doi:10.1364/ol.448326

47. Wang B, Yang Z, Sun S, Yi X. Radio-frequency line-by-line Fourier synthesis based on optical soliton microcombs. *Photon Res* (2022) 10:932. doi:10.1364/prj.450103